Metastable states of D_2^- observed by foil-induced Coulomb explosion imaging

P. Herwig,[1] D. Schwalm,[1,2] M. Čížek,[3] R. Golser,[4] M. Grieser,[1] O. Heber,[2] R. Repnow,[1] A. Wolf,[1] and H. Kreckel[1,*]

[1]*Max-Planck-Institut für Kernphysik, 69117 Heidelberg, Germany*

[2]*Department of Particle Physics, Weizmann Institute of Science, Rehovot 76100, Israel*

[3]*Charles University Prague, Faculty of Mathematics and Physics, Institute of Theoretical Physics, 180 00 Praha 8, Czech Republic*

[4]*Universität Wien, Fakultät für Physik–Isotopenforschung, 1090 Wien, Austria*

(Received 27 April 2013; published 24 June 2013)

In recent years it was demonstrated that the negative hydrogen molecular ions H_2^- and D_2^- exist in long-lived states with lifetimes exceeding 1 μs (H_2^-) and 1 ms (D_2^-). These metastable ions exhibit very large internuclear distances and possess high angular momenta, which stabilizes them against autodetachment. Here we present the results of a foil-induced Coulomb explosion imaging experiment that allows for the measurement of the rovibrational wave functions of the metastable D_2^- ions. We compare our results to previous predictions from a nonlocal resonance theory. Our measurements do not confirm the discrepancy between experiment and theory that was inferred from previous photofragmentation studies. In fact, we find good agreement between the experiment and calculated wave functions for the most long-lived states with rotational quantum numbers $J = 37$ and 38.

DOI: 10.1103/PhysRevA.87.062513 PACS number(s): 33.15.Dj, 79.77.+g

I. INTRODUCTION

Molecular ions play important roles in many fields, from atmospheric physics to combustion and interstellar chemistry. While positive molecular ions are being studied in great detail by many groups around the world, data on negative molecular ions are comparatively sparse. One of the obstacles may be the fact that negative ions rarely have more than one bound electronic state [1], which renders electronic spectroscopy impossible. In many cases the only available data on negative ions are the electron affinities, which have been derived from photodetachment experiments or collision studies.

Nevertheless, negative ions have attracted a lot of attention recently, as the first detection of an anion in interstellar space [2] has prompted many questions on their abundance in different interstellar environments. Negative ions have also been found to play an important role in the early Universe [3], and it is clear that a thorough understanding of negative ion reactions will be crucial for the operation and control of nuclear fusion devices.

The simplest molecular anion is the negative hydrogen molecule H_2^-. Early reports on detections of H_2^- by mass spectrometry date back to the 1950s and 1970s [4–6]. However, in 1963, Taylor and Harris [7] performed calculations that showed that the lowest $^2\Sigma_u^+$ state of H_2^- is unstable with respect to autodetachment at short internuclear distances. Subsequent theoretical considerations by Bardsley *et al.* [8] yielded lifetimes on the order of 10^{-16} s, much too short for the ions to be observable. Furthermore, dedicated experiments by Bae *et al.* in 1984 [9] cast doubts on the early detections since they did not yield any evidence for negative hydrogen molecules, while they successfully produced other molecular anions.

The first unambiguous identification of metastable H_2^- and D_2^- was achieved at the VERA accelerator in 2005 [10] and verified by highly accurate mass spectrometry [11]. Subsequent ion trap measurements revealed lifetimes up to $\sim$8 μs for H_2^- and $\sim$1.9 ms for D_2^- [12].

A theoretical description of the long-lived anionic states was offered already in [10] and further refined by Čížek *et al.* in [13]. Initial calculations of the same group within the nonlocal resonance model had aimed at an understanding of H_2^- transient states in associative detachment (AD: $H^- + H \rightarrow H_2^- \rightarrow H_2 + e^-$) and dissociative attachment (DA: $e^- + H_2 \rightarrow H_2^- \rightarrow H + H^-$) reactions [14], and they showed excellent agreement with recent measurements of the AD process [3,15]. Within the same model, H_2^- and D_2^- were found to be able to form metastable states when the molecule rotates strongly, thereby increasing the distance between the nuclei and keeping the ion from entering the region of rapid autodetachment at short internuclear distances. A refined calculation [13] was able to reproduce the measured lifetimes and predicted the most long-lived states to be characterized by rotational quantum numbers $J = 27$ for H_2^- and $J = 37$–38 for D_2^-.

To verify the calculations and to shed light on the structure of these fundamental anions, a foil-induced Coulomb explosion imaging (CEI) measurement was carried out with metastable H_2^- [16]. The CEI experiment allows for a direct imaging of the nuclear wave function of molecular ions [17]. In the case of H_2^-, where only the longest lived state with $J = 27$ and vibrational quantum number $v = 0$ is expected to survive the transport from the ion source to the experiment, the outcome of the CEI measurements showed excellent agreement with the calculated wave function of Čížek *et al.* [13,14], thereby confirming the vibrational quantum number $v = 0$ and the expected large average distance between the two protons of ~ 6 a.u. Moreover, by imaging also the autodetachment product H_2, it was possible to get an independent confirmation of the predicted rotational quantum number $J = 27$ of the metastable state.

In the meantime, a complementary characterization of metastable D_2^- ions had been carried out by Lammich *et al.* [18]. In their experiments, a fast D_2^- beam was ionized by pulsed laser light and the kinetic energy released in the subsequent dissociation of the neutral D_2 was analyzed. The

*Corresponding author: holger.kreckel@mpi-hd.mpg.de

authors concluded that the observed kinetic energy release spectra deduced from these photofragmentation studies show a clear discrepancy with calculated energy distributions based on the results of Čížek *et al.* While theory predicts that only states with $J = 37$ and 38 live long enough to survive the flight times of $\sim 10\ \mu$s between ion source and experiment, they inferred from their results that theory is overestimating the angular momenta of the most long-lived states of D_2^- by several $\hbar$.

Here we present a foil-induced Coulomb explosion imaging experiment with metastable D_2^- ions to perform an independent and stringent test of the molecular wave functions connected with these long-lived states. The paper is organized as follows. In Sec. II we describe the experimental setup. In Sec. III an outline of the Coulomb explosion process is given together with a comparison of semiclassical and quantum-mechanical simulations of the kinetic energy release distributions. In Sec. IV we present the results of the experiment, and we provide a summary in Sec. V. In the Appendix we reevaluate the results from the photodissociation experiment by Lammich *et al.* [18].

II. EXPERIMENTAL SETUP

We have used the Coulomb explosion imaging (CEI) setup [19] at the Max Planck Institute für Kernphysik in Heidelberg, Germany. The D_2^- ions were extracted from an off-axis duoplasmatron ion source. The ion source produced several μA at mass 2 (D^-), while the target mass 4 beam (D_2^-) was much weaker, typically on the order of $\sim$50 pA. The ions were injected into a linear radiofrequency accelerator and accelerated to a kinetic energy of 1.92 MeV. At these energies, the distance from the accelerator to the CEI beamline translates into a flight time of $\sim 10\ \mu$s. In the CEI beamline, the ion beam is collimated by two movable circular apertures. To create a pencil beam, the apertures are set to either 1 or 1.5 mm (both values were used during the experiment). A sketch of the CEI beamline is given in Fig. 1.

The collimated ion beam is directed at the target foil, which is made out of diamond-like carbon (DLC) with a nominal thickness of $\sim$5 nm [20]. Inside the target foil all electrons are stripped off upon entry within 10^{-16} s.

Once the electrons are gone, the Coulomb explosion process sets in and the potential energy that is stored in the

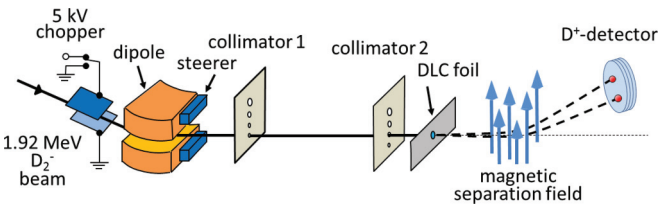

FIG. 1. (Color online) Schematic of the CEI beamline. The D_2^- beam is defined by two collimators and impinges on a DLC stripping foil that is supported by a nickel mesh. Via a magnetic separation field, the two D^+ fragments are selected and guided toward a 3D imaging detector. Between the DLC foil and the detector, the fragments gain a distance of a few centimeters due to the Coulomb explosion process. A fast beam chopper ensures the detection of single-molecule events by blocking the D_2^- beam after the first impact at the detector.

remaining $D^+ + D^+$ configuration is rapidly converted into kinetic energy. The nuclei start to drift apart, and after a flight distance of $\sim$4 m they are recorded by a three-dimensional imaging detector. At this time they have gained distances of up to a few centimeters. A magnetic separation field between the target foil and the detector can be used to mass select the respective fragments in experiments with heteronuclear molecules. In the present experiment, the magnetic field was used to deflect both D^+ fragments onto the CEI detector and to discriminate against rare neutral fragments which can also emerge from the target foil.

The events are recorded on a single-molecule basis. To this end, the particle rate is kept low (on the order of $\sim$1 kHz) and a fast high-voltage chopper at the beginning of the CEI beamline prevents molecules from reaching the detector after the first fragment impact is detected. The CEI detector system has been described in detail elsewhere [19]. It features multihit capability with a spatial resolution of $\sim$0.1 mm and a time resolution of $\sim$130 ps.

III. DESCRIPTION OF THE COULOMB EXPLOSION PROCESS

Figure 2 shows an illustration of the Coulomb explosion principle. As the stripping process in the DLC foil is fast as

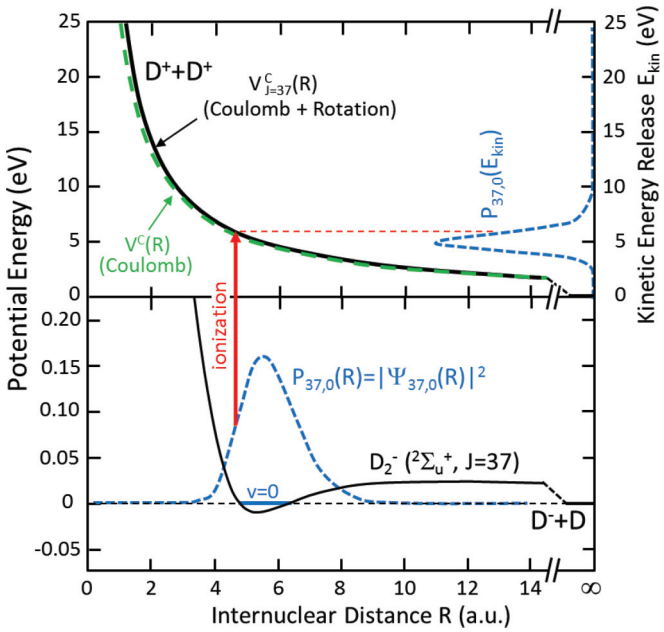

FIG. 2. (Color online) Principle of Coulomb explosion imaging. The solid line in the lower panel shows the $^2\Sigma_u^+$ ($J = 37$) potential energy curve of D_2^- [13], which leads asymptotically to $D^- + D$. Also plotted is the vibrational ground state together with the corresponding distance distribution $P_{37,0}(R)$ determined by the square of the rovibrational wave function for $J = 37, v = 0$ (dashed blue line). Assuming an instantaneous stripping process, the two positively charged deuterons find themselves sitting on the potential energy curve $V^C_{J=37}(R)$ displayed in the upper panel, which is given by the sum of the Coulomb potential and the centrifugal potential for $J = 37$. The potential energy of the two deuterons is then transformed into kinetic energy $E_{\rm kin}$, which leads to a kinetic energy release distribution $P_{37,0}(E_{\rm kin})$ shown by the dashed blue line.

compared to typical time scales of vibrational and rotational motion of the D_2^- molecule, the two deuterons—separated at a distance R at the moment of ionization—suddenly find themselves located on the potential energy curve given by the sum of the Coulomb potential $V^C(R) = e^2/R$ and the centrifugal potential $V_J(R) = \hbar^2/(2\mu R^2)J(J+1)$, where μ stands for the reduced mass. The two deuterons start drifting apart and the total energy $E = V_J^C(R) = V^C(R) + V_J(R)$ is eventually transformed into kinetic energy $E_{\rm kin}$. The resulting kinetic energy release (KER) distribution is given by

$$P_{J,v}(E_{\rm kin})\,dE_{\rm kin} = \left|\int_0^\infty \Psi^*_{J,v}(R)\Psi^{\rm C}_J(R,E_{\rm kin})dR\right|^2 dE_{\rm kin}, \quad (1)$$

where $\Psi_{J,v}(R)$ denotes the rovibrational wave function of the D_2^- ion with parameters J and v given by the rotational and vibrational quantum numbers, respectively. Moreover, $\Psi^{\rm C}_J(R,E_{\rm kin})$ denotes the continuum wave function of the two dissociating D^+ ions with total kinetic energy $E_{\rm kin}$ and rotational angular momentum J, which is the solution of the one-dimensional Schrödinger equation

$$\left\{\frac{d^2}{dR^2} + \frac{2\mu}{\hbar^2}\left[E_{\rm kin} - V_J^C(R)\right]\right\}\Psi^{\rm C}_J(R,E_{\rm kin}) = 0. \quad (2)$$

Note that in writing down Eq. (1), we neglected for the time being any modifications of the KER distribution caused by the interaction of the two separating deuterons in the target foil. Furthermore, we make the usual assumption that the rotational angular momentum of the molecule is not changed by the stripping process.

The wave functions obtained within the nonlocal resonance framework [13] for vibrational states with $v = 0$ and 1, which are the only two states supported by the $D_2^-(^2\Sigma_u^+, J = 37)$ potential, are plotted in Fig. 3(a), while the corresponding KER distributions obtained with the aid of Eq. (1) are shown in Fig. 3(b). The exceptionally large average distance of ~6 a.u. between the two nuclei in these states results in relatively small kinetic energies of around 5 eV.

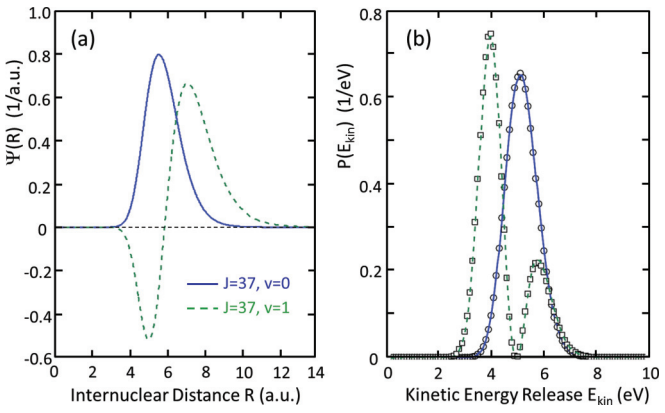

FIG. 3. (Color online) Comparison of the quantum-mechanical and semiclassical treatment of the Coulomb explosion process. (a) Rovibrational wave function of the $^2\Sigma_u^+(J = 37, v = 0)$ state (blue solid line) and of the $^2\Sigma_u^+(J = 37, v = 1)$ state (dashed green line) as calculated in the nonlocal resonance framework [13]. (b) Corresponding KER distributions calculated using the quantum-mechanical Coulomb wave functions (lines) and applying the semiclassical approximation (symbols).

However, as long as the Coulomb energy is dominating the kinetic energy release when compared to the vibrational and rotational energy of the molecule, the evaluation of Eq. (1) can be simplified by approximating the continuum wave function $\Psi^{\rm C}_J(R,E_{\rm kin})$ by the properly normalized [21] position eigenstates, that is,

$$\Psi^{\rm C}_J(R,E_{\rm kin}) \approx \sqrt{\left|\frac{dR(E_{\rm kin})}{dE_{\rm kin}}\right|}\,\delta(R - R(E_{\rm kin})), \quad (3)$$

where δ denotes Dirac's δ function and $R(E_{\rm kin})$ is implicitly given by $E_{\rm kin} = V_J^C(R)$. This leads to the well-known semiclassical approximation employed in most CEI experiments,

$$P_{J,v}(E_{\rm kin})\,dE_{\rm kin} \approx |\Psi_{J,v}(R)|^2\left|\frac{dR}{dE_{\rm kin}}\right|dE_{\rm kin}. \quad (4)$$

Equation (4) shows that the KER distribution can be considered within this approximation to be the mirror image of the square of the rovibrational wave function, obtained by projecting $|\Psi_{J,v}(R)|^2$ onto the potential energy curve $V_J^C(R)$ (see Fig. 2). The semiclassical approximation of the KER distributions for the two wave functions shown in Fig. 3(a) is compared in Fig. 3(b) to the exact quantum-mechanical results. As observed already in the case of H_2^- [16], the agreement between the two methods is still excellent despite the unusually large rotational angular momentum.

The semiclassical approximation is the basis of a well-established Monte Carlo simulation program [22,23], which treats the Coulomb explosion process in discrete time steps and which allows us to take into account multiple scattering and charge exchange processes of the separating ions inside the foil as well as the magnetic separation field and the detector resolution. In previous work, the CEI simulation code has shown excellent agreement with observed KER distributions, in particular also for hydrogenic molecules [24,25]. While in these studies the rotational energy carried by the molecules was usually very small and could thus be neglected in view of the dominant Coulomb energy, in the present case the initial rotational energies the nuclei possess due to the molecular rotation were explicitly taken into account by giving each deuteron an initial center-of-mass velocity [16],

$$v_J(R) = \frac{\hbar}{2\mu R}\sqrt{J(J+1)}, \quad (5)$$

oriented perpendicular to the molecular as well as rotational axis. The further time development of the Coulomb explosion then follows the usual procedure of calculating the trajectories of the separating ions under the influence of the mutual Coulomb force.

IV. RESULTS AND DISCUSSION

In Fig. 4, the measured KER distribution resulting from the Coulomb explosion of metastable D_2^- ions is shown. The distribution is centered around ~5 eV, corresponding to a relatively "soft" explosion or large internuclear separation (for comparison, the KER distribution for H_2 is centered around ~16 eV [16]). Several measures are taken to suppress unwanted background: Only events with two hits on the

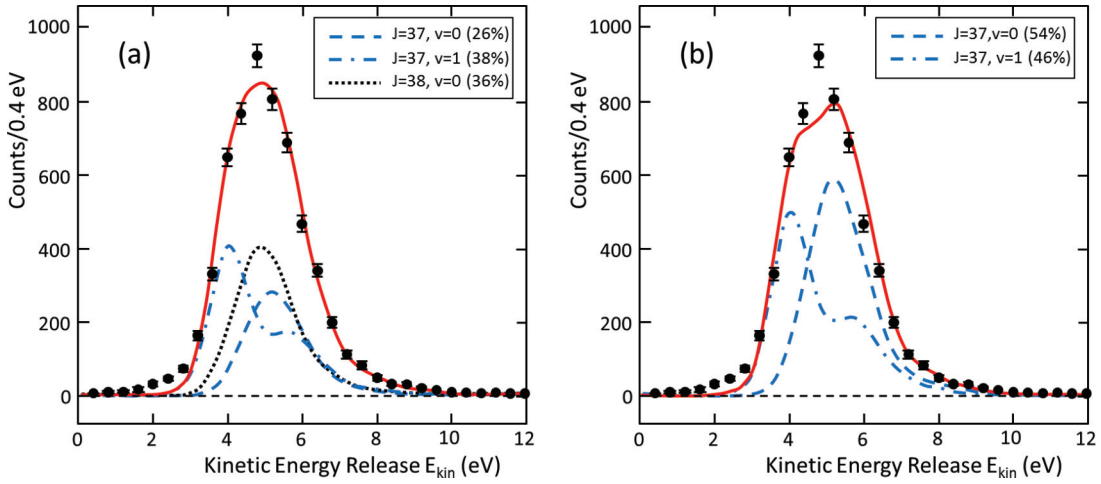

FIG. 4. (Color online) Kinetic energy release (KER) distributions measured for D_2^- after all cuts. The error bars show the uncertainty resulting from the counting statistics on a 1σ level. The uncertainty in the KER is on the order of the size of the solid dots. The left panel (a) shows a fit (solid red line) using the simulated distributions for the three predicted metastable states that are long-lived enough to be detectable. These states are $(J = 37, v = 0)$, $(J = 37, v = 1)$, and $(J = 38, v = 0)$. For the simulation, the calculated wave functions of Čížek *et al.* [13] were used as input of the CEI Monte Carlo code (see text for details). The right panel 4(b) shows a fit (solid red line) using only two wave functions, namely $(J = 37, v = 0)$ and $(J = 37, v = 1)$. The choice of these two states is motivated by the measurements of Lammich *et al.* [18], who used the same type of ion source that was used for the present work and did not observe significant population in the $(J = 38, v = 0)$ state. The populations of the individual states were used as fit parameters; the resulting populations are given in the insets. The broken lines show the respective simulated KER distributions for the individual wave functions.

detector are accepted. The center-of-mass (CMS) distribution of the two fragments in the detector plane has been calculated and only events with a CMS lying within a 0.5 mm radius from the central spot of the distribution have been accepted for the plot. This CMS cut is a standard procedure that is used to clean the CEI data sample from large-angle scattering events, remaining random coincidences, and from detector noise. Furthermore, all events with $\sin\alpha > 0.48$ were rejected, where α stands for the angle between the detector plane and the molecular axis. This cut discards all events that have a small spatial distance in the detector plane. This selection criterion very efficiently eliminates the so-called "wake effect" that is caused by the electronic excitation of the target foil [26] induced by the passage of the swift ions. This effect can influence the ion trajectories for events where one of the fragments trails the other one inside the target foil.

The measured distributions are compared to simulated distributions based on the wave functions of Čížek *et al.* [13] in Fig. 4. We applied the same cuts that were used for the experimental data to the simulated data. According to the theoretical predictions, three states have lifetimes $\gtrsim 10$ μs and thus live long enough to survive the flight distance between the ion source and the experimental setup. These are the states $(J = 37, v = 1)$, $(J = 37, v = 0)$, and $(J = 38, v = 0)$ with lifetimes of 16 μs, 61 μs, and 2.1 ms, respectively. These lifetimes are in reasonable agreement with the three decay times observed in the experiment of Heber *et al.* [12], which were found to be (23 ± 3) μs, (84 ± 3) μs, and (1.89 ± 0.08) ms, respectively. When all three states are included in the fit of the experimental distribution [see Fig. 4(a)], a good representation of the data is obtained when adjusting the relative intensities of the three distributions. In particular, the center of the measured distribution is close to the predicted centers of the $(J = 37, v = 0)$ and $(J = 38, v = 0)$ states. The small deviations around 2.5 eV are probably caused by residual gas collisions in the CEI beamline due to imperfect vacuum conditions at the time of the experiment. These collisions can lead to molecular breakups before the target foil. Since in this case the particles will start to drift apart before they get ionized inside the foil, the kinetic energy release from the Coulomb explosion is reduced. However, simulations have shown that this background process is not expected to affect the main foil-induced distribution.

In our previous experiments with H_2^-, the decay of the anions along the straight beam path after the last bending magnet seemed to produce predominantly neutral H_2 molecules. We verified this by introducing an additional magnetic field in front of the target foil to deflect all charged particles and record the breakup of the neutral molecules [16]. Analysis of the neutral flux and the beam lifetime revealed the autodetachment channel of H_2^- to be the dominant decay path. In the case of D_2^-, however, we found the number of neutral autodetachment products in the beam to be too small to be safely distinguishable from background events. Due to the longer lifetimes of the D_2^- states in the ion beam, our detection limit is not excluding the possibility that all states decay predominantly by electron detachment. On the other hand, it may well be that the shortest-lived state in the beam with a lifetime of 23 μs is decaying by dissociation, as suggested by the measurement of Heber *et al.* [12].

The intensities obtained in the three-level fit of our data indicate that the relative populations of the states at the time the ions left the duoplasmatron source were almost equal, similar to what has been observed by Heber *et al.* [12], where a sputter ion source was used to produce D_2^-. Although the formation process of the D_2^- anions is not really understood,

it seems that the different natural widths of the D_2^- states are not reflected in their relative populations. On the other hand, Lammich *et al.* [18] used lifetime data of a stored D_2^- beam to infer time-dependent populations of the different D_2^- states. They concluded that the longest-lived state—predicted to be $(J = 38, v = 0)$—had a very small initial population of only 0.6%, while the two other long-lived states $(J = 37, v = 0)$ and $(J = 37, v = 1)$ were almost equally populated. Since in their study a duoplasmatron ion source was used—the same type of source as in the present work—it is interesting to verify whether such a small population of the $(J = 38, v = 0)$ state is consistent with our data. A fit of our measured KER distribution allowing only the $(J = 37, v = 0)$ and $(J = 37, v = 1)$ state to contribute is displayed in Fig. 4(b). While a negligible population of the $(J = 38, v = 0)$ state is not really excluded, we do get a noticeably improved fit of our data if we include the $(J = 38, v = 0)$ state as shown in Fig. 4(a).

The discrepancy between theory and experiment that was inferred from a previous photofragmentation experiment on D_2^- by Lammich *et al.* [18] is not observed here. They concluded that the energy release distributions they observed after photoionization with 532 nm laser pulses cannot be explained by wave functions proposed by Čížek *et al.* for these states. As almost all the energy released in the photofragmentation process of D_2^- stems from the rotational motion rather than from the potential energy, the resulting KER distributions are determined not only by the R dependence of the wave functions but in particular also by J; the authors thus interpreted their findings by suggesting that theory is overestimating the rotational angular momenta connected with these metastable states and proposed J values around $J = 33$ instead of $J = 37$–38. In CEI measurements, on the other hand, the kinetic energy release is dominated by the Coulomb potential and therefore is mainly sensitive to the R dependence of the rovibrational wave function, for which we find good agreement between theory and experiment. Because of the different sensitivities of the two experiments on R and J, one thus cannot refute for the time being the conclusion of Lammich *et al.* Nevertheless, their conclusion remains puzzling in view of the previous CEI results for H_2^- [16], where not only the R dependence but also the rotational angular momentum of the predicted metastable $(J = 27, v = 0)$ state agreed well with theory.

To understand in more detail the disagreement between theory and data claimed by Lammich *et al.* [18], we tried to verify their conclusion by recalculating the kinetic energy distributions expected on the basis of the theoretical wave functions obtained by Čížek *et al.* [13]. As outlined in the Appendix, we cannot reproduce the discrepancy. On the contrary, allowing *both* possible ionization channels, $D_2^-(^2\Sigma_u^+) + \hbar\omega \rightarrow D_2(X\,^1\Sigma_g^+) + e^-$ and $\rightarrow D_2(b\,^3\Sigma_u^+) + e^-$, to contribute, we can obtain reasonable descriptions of their observed KER distributions by using state populations inferred from their decay rate measurement and adjusting only the ratio between the contributions of the $X\,^1\Sigma_g^+$ and $b\,^3\Sigma_u^+$ channel. In fact, we find that the photofragmentation data of Lammich *et al.* [18] limit the rotational angular momenta of the potential energy curves, along which the photoinduced dissociation of the D_2^- states with lifetimes of ~ 20 and ~ 80 μs occurs, to $J = 36$, thereby confirming the predicted high rotational angular momenta of these states.

V. SUMMARY

We have performed foil-induced Coulomb explosion measurements with a beam of metastable D_2^- ions. The measured kinetic energy distributions center around a small energy release of ~ 5 eV, directly confirming the predicted large internuclear distance of this simple negative anion. The distribution is in good agreement with a previous nonlocal resonance theory [13]. We find that a fit using the three D_2^- states with the longest predicted lifetimes, namely $(J = 37, v = 0)$, $(J = 37, v = 1)$, and $(J = 38, v = 0)$, reproduces the experiment well.

The main discrepancy between theory and experiment claimed in the previous photodissociation experiment seems to be resolved. We believe that the claim was based on the simplifying assumption that only one of the possible fragmentation channels is contributing to the measured kinetic energy distributions. In particular, we find that their data confirm the predicted high rotational angular momenta of the D_2^- states with lifetimes > 10 μs.

In light of the foil-induced CEI results, for both H_2^- [16] and D_2^-, and the excellent agreement between experiment and theory for the AD process, where H_2^- and D_2^- serve as intermediate states [3,15,27,28], it is apparent that great strides have been made toward a better understanding of this most fundamental molecular anion.

ACKNOWLEDGMENTS

We thank the accelerator staff at the Max Planck Institute for Nuclear Physics, especially M. König and M. Trebis, for their expert tuning of the elusive D_2^- beam. We acknowledge support from the Max Planck Society. H.K. was supported by the European Research Council under Grant Agreement No. StG 307163. M.C. was supported by the grant agency of the Czech Republic project No. GACR 208/10/1281. D.S. acknowledges support from the Weizmann Institute through the Joseph Meyerhoff program.

APPENDIX: PHOTOFRAGMENTATION OF D_2^-

Lammich *et al.* [18] performed photofragmentation experiments on D_2^- by crossing a 20 keV beam of D_2^- with 532 nm laser pulses and observing the two dissociating deuteriums using an MCP detector equipped with a phosphor screen. While the spatial distance between the two coincident particles was determined from the CCD picture of the phosphor screen, the impact time difference between them was deduced from the time traces of the analog MCP signal recorded with a digital storage oscilloscope. The reconstructed kinetic energy release is reported to be determined in this way with a 1σ resolution of $\delta E_{\rm kin}/E_{\rm kin} \sim 5\%$. The experiments were performed in a single pass setup after a flight time of 10 μs and after 26 and 107 μs by storing the anions in a storage ring.

An overview of the relevant potential energy curves is shown in Fig. 5. Assuming the photodetachment does not change the rotational angular momentum J, two ionization channels are open, which leave the two deuteriums either on the D_2 ground-state potential energy curve $V_{X\,^1\Sigma_g^+}(R)$, or on the D_2 excited potential energy curve $V_{b\,^3\Sigma_u^+}(R)$. Both potential energy curves are shifted upward by the centrifugal

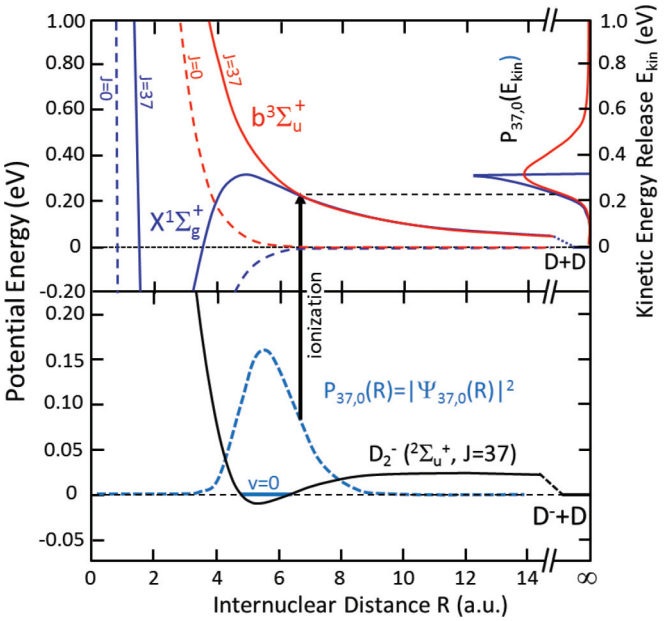

FIG. 5. (Color online) Potential energy curves relevant for the photodissociation experiment of D_2^- performed by Lammich *et al.* [18]. Photodetachment of an electron from the $(X\,^2\Sigma_u^+, J = 37)$ state results in a neutral D_2 molecule being either on the $(b\,^3\Sigma_u^+, J = 37)$ or $(X\,^1\Sigma_g^+, J = 37)$ potential energy curve, assuming the rotational angular momentum to be conserved in the detachment process. The dissociation of the D_2 then leads to kinetic energy distributions indicated at the right-hand side of the upper panel.

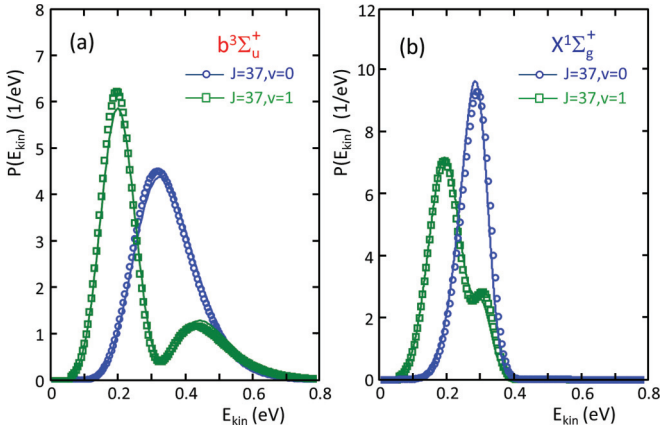

FIG. 6. (Color online) Comparison of the kinetic energy release distributions calculated using Eq. (A1) (solid lines) to those using the semiclassical approximation (symbols) for photofragmentation of the $(J = 37, v = 0)$ and $(J = 37, v = 1)$ state of D_2^- via (a) the $(b\,^3\Sigma_u^+, J = 37)$ and (b) the $(X\,^1\Sigma_g^+, J = 37)$ channel. The distributions are folded with the experimental energy resolution.

potential connected with the rotational angular momentum J. The resulting kinetic energy distributions are indicated on the right-hand side of the upper panel of Fig. 5; while the $(b\,^3\Sigma_u^+, J)$ distribution reflects the total D_2^- wave function, the $(X\,^1\Sigma_g^+, J)$ distribution is cut off at the energy $E_J^{\max}$, given by the maximum of the $(X\,^1\Sigma_g^+, J)$ potential energy curve, which occurs around $R \approx 5$ a.u.

As indicated in Fig. 5, the kinetic energy release is dominated in this case by the energy stored in the rotational motion, in contrast to the situation found in foil-induced CEI experiments. We therefore investigated, in a first step in our attempts to understand the results of Lammich *et al.*, the validity of the semiclassical approximation used in Ref. [18]. Following the same line of reasoning as in Sec. III, the kinetic energy distribution is given within the dipole approximation by

$$P^n_{J,v}(E_{\rm kin}) \propto \left| \int_0^\infty \Psi^*_{J,v}(R)\mu^n_J(R)\Psi^n_J(R, E_{\rm kin})dR \right|^2, \quad \text{(A1)}$$

where $\mu^n_J(R)$ denotes the electronic transition dipole moment and n denotes the final electronic state ($X\,^1\Sigma_g^+$ or $b\,^3\Sigma_u^+$). The continuum wave function $\Psi^n_J(R, E_{\rm kin})$ is now the solution of Eq. (2) with the potential V_J^C being replaced by $V_{J,n}(R) = V_n(R) + V_J(R)$. The semiclassical approximation to Eq. (A1) is again obtained by replacing $\Psi^n_J(R, E_{\rm kin})$ by the normalized position eigenfunction given by Eq. (3), where $R(E_{\rm kin})$ is now implicitly given by $E_{\rm kin} = V_{J,n}(R)$, with R restricted to $R \geqslant R_J^{\max}$ for the dissociation via the $(X\,^1\Sigma_g^+, J)$ potential energy curve. Here $R_J^{\max}$ denotes the internuclear distance where the $(X\,^1\Sigma_g^+, J)$ potential energy curve is going through a maximum.

A comparison of the kinetic energy distributions resulting from Eq. (A1) to those obtained within the semiclassical approximation is shown in Fig. 6 for the two rovibrational states with $(J = 37, v = 0)$ and $(J = 37, v = 1)$. To calculate the distributions, we used the potential energy curves $V_n(R)$ tabulated in Ref. [29] and assumed—as in Ref. [18]—the electronic transition dipole moment to be R-independent. The distributions were folded with the experimental energy resolution and normalized to unity. The differences between the exact and approximate distributions are now more pronounced than in foil-induced CEI experiments, in particular also for the $X\,^1\Sigma_g^+$ channel [see Fig. 6(b)]. In contrast to the semiclassical approach, where the enhancement of the KER distribution at $E_J^{\max}$ is caused by the divergence of $|dR/dE_{\rm kin}|$, in the quantum-mechanical description the least bound vibrational states supported by the $(X\,^1\Sigma_g^+, J)$ potential energy curves have large tunneling probabilities, and thus interfere strongly with the continuum. This leads to pronounced resonance-like structures in the corresponding KER distributions, which are only partially damped out by the finite energy resolution. For $J = 37$, in particular, the $v = 9$ vibrational state lies by chance very close to $E_{37}^{\max}$ and thereby acquires a tunneling width of several meV. This results in a strong increase of the KER distributions around $E_{37}^{\max}$ similar to what is obtained in the semiclassical treatment. In any case, the accuracy of the semiclassical approximation is still tolerable; its use in Ref. [18] cannot be the cause of the failure to reproduce the fragmentation data using the predicted wave functions of Ref. [13].

In a next step, we calculated the KER distribution for a D_2^- ensemble containing the three longest-lived states using the quantum-mechanical approach and relative populations of the states deduced by Lammich *et al.* from the measured storage time dependence of the D_2^- beam (see Table I in [18]). The distribution derived for a flight time of 10 μs and including *both* fragmentation channels is compared to the distribution

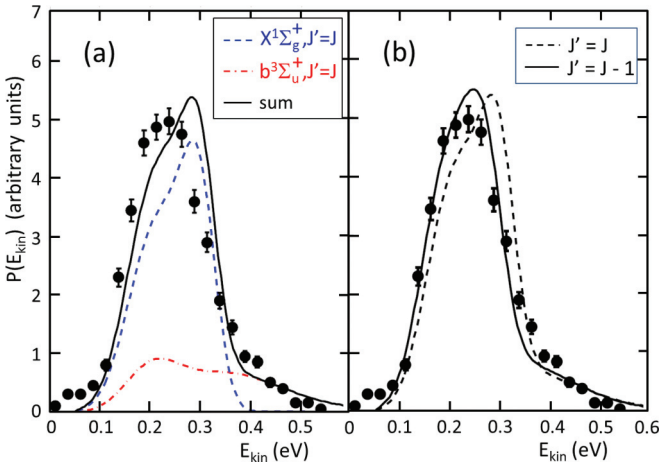

FIG. 7. (Color online) Kinetic energy release distribution observed by Lammich *et al.* [18] in their photofragmentation experiment of a D_2^- beam 10 μs after the ion production (dots with error bars, redrawn from Fig. 6 of Ref. [18]). The experimental KER distribution is compared to calculated distributions, which are based on the wave functions $\Psi_{J,v}(R)$ of Ref. [13] and on populations $Q_{J,v}$ deduced in Ref. [18] to be $Q_{37,0} : Q_{37,1} : Q_{38,0} = 54 : 45 : 1$. The theoretical distributions were folded with the experimental energy resolution. (a) The blue (dashed) and red (dashed-dotted) lines show the KER distributions resulting from the dissociation via the $(X\,^1\Sigma_g^+, J')$ and $(b\,^3\Sigma_u^+, J')$ potential energy curve, respectively, assuming $J' = J$. The black solid line represents the sum of the two contributions. (b) Summed KER distributions assuming $J' = J - 1$ (solid line) and $J' = J$ (dashed line). In (a) and (b) the relative intensities of the two dissociation channels were adjusted to $I(X\,^1\Sigma_g^+) : I(b\,^3\Sigma_u^+) = 70 : 30$.

measured by Lammich *et al.* in Fig. 7(a). The only free parameter in the calculation was the relative contribution of the two fragmentation channels. Surprisingly, we find that the main features of the measured distribution are reasonably well accounted for, considering that no attempt was made to adjust any of the other input parameters or input assumptions. We therefore believe that the conclusion reached by Lammich *et al.*, namely that the current theoretical description of metastable D_2^- states clearly needs modification, is not justified. It appears that the missing contribution from the $X\,^1\Sigma_g^+$ fragmentation channel caused the deviation between the calculated KER distribution and the experimental results.

The observed kinetic energy distribution is in fact dominated by the $(X\,^1\Sigma_g^+, J')$ fragmentation channel, the high-energy edge of which is controlled by the maximum of the potential energy curve, $E_{J'}^{\max}$, rather than by the detailed R dependence of the contributing wave functions, in contrast to the low-energy edge, which is determined by the R behavior of the wave function at large internuclear distances. The position of the high-energy edge of the $(X\,^1\Sigma_g^+, J')$ distribution thus provides a sensitive, almost model-independent access to the rotational angular momenta J' of the involved dissociation curves. In an attempt to exploit this sensitivity, we compare in Fig. 7(b) the experimental distribution to a KER distribution derived using the same wave functions and populations as in Fig. 7(a) but assuming $J' = J - 1$. The resulting distribution, which is downshifted by ~ 22 meV as compared to the $J' = J$ distribution, is found to be in almost perfect accord with the data. Moreover, a similar agreement is obtained under these assumptions for the KER distributions observed in [18] after storage times of 26 and 107 μs. On the other hand, the kinetic energy distribution calculated by replacing the $J = 37$ wave functions by the corresponding rovibrational wave functions predicted for $J = 36$, and assuming $J' = J$, grossly fails to explain the measured low-energy edge of the distribution measured at 10 μs.

As a further reduction to $J' = J - 2$ leads to KER distributions which start to fail to describe the measured upper edges, we conclude that the experimental findings of Lammich *et al.* [18] are consistent with the assumption that the photoinduced dissociation of the D_2^- states with lifetimes of ~ 20 μs and ~ 80 μs proceeds via potential energy curves with $J' \approx 36 \pm 1$, thereby supporting the high rotational angular momenta predicted by Čížek *et al.* [13] for these states. We find that the predicted R dependencies of the corresponding wave functions are in accord with the photofragmentation data. Further analysis, however, would require more detailed calculations of the photoinduced cross sections to the two final electronic channels, including in particular the R dependence of the electronic transition dipole moment and the possibility of transitions with $|J' - J| \neq 0$.

[1] D. J. Pegg, Rep. Prog. Phys. **67**, 857 (2004).
[2] M. C. McCarthy, C. A. Gottlieb, H. Gupta, and P. Thaddeus, Astrophys. J. **652**, L141 (2006).
[3] H. Kreckel, H. Bruhns, M. Čížek, S. C. O. Glover, K. A. Miller, X. Urbain, and D. W. Savin, Science **329**, 69 (2010).
[4] V. I. Khvostenko and V. M. Dukel'Skii, Sov. Phys. JETP **7**, 709 (1958).
[5] R. Hurley, Nucl. Instrum. Methods **118**, 307 (1974).
[6] W. Aberth, R. Schnitzer, and M. Anbar, Phys. Rev. Lett. **34**, 1600 (1975).
[7] H. S. Taylor and F. E. Harris, J. Chem. Phys. **39**, 1012 (1963).
[8] J. N. Bardsley, A. Herzenberg, and F. Mandl, Proc. Phys. Soc. **89**, 305 (1966).
[9] Y. K. Bae, M. J. Coggiola, and J. R. Peterson, Phys. Rev. A **29**, 2888 (1984).
[10] R. Golser, H. Gnaser, W. Kutschera, A. Priller, P. Steier, A. Wallner, M. Čížek, J. Horáček, and W. Domcke, Phys. Rev. Lett. **94**, 223003 (2005).
[11] H. Gnaser and R. Golser, Phys. Rev. A **73**, 021202 (2006).
[12] O. Heber, R. Golser, H. Gnaser, D. Berkovits, Y. Toker, M. Eritt, M. L. Rappaport, and D. Zajfman, Phys. Rev. A **73**, 060501 (2006).
[13] M. Čížek, J. Horácek, and W. Domcke, Phys. Rev. A **75**, 012507 (2007). The wave functions obtained with the unperturbed $^2\Sigma_u^+$ potential are used in the present work.

[14] M. Čížek, J. Horácek, and W. Domcke, J. Phys. B **31**, 2571 (1998).
[15] K. A. Miller, H. Bruhns, J. Eliášek, M. Čížek, H. Kreckel, X. Urbain, and D. W. Savin, Phys. Rev. A **84**, 052709 (2011).
[16] B. Jordon-Thaden, H. Kreckel, R. Golser, D. Schwalm, M. H. Berg, H. Buhr, H. Gnaser, M. Grieser, O. Heber, M. Lange, O. Novotny, S. Novotny, H. B. Pedersen, A. Petrignani, R. Repnow, H. Rubinstein, D. Shafir, A. Wolf, and D. Zajfman, Phys. Rev. Lett. **107**, 193003 (2011).
[17] Z. Vager, R. Naaman, and E. P. Kanter, Science **244**, 426 (1989).
[18] L. Lammich, L. H. Andersen, G. Aravind, and H. B. Pedersen, Phys. Rev. A **80**, 023413 (2009).
[19] R. Wester, F. Albrecht, M. Grieser, L. Knoll, R. Repnow, D. Schwalm, A. Wolf, A. Baer, J. Levin, Z. Vager, and D. Zajfman, Nucl. Instrum. Methods Phys. Res. A **413**, 379 (1998).
[20] J. Levin, L. Knoll, M. Scheffel, D. Schwalm, R. Wester, A. Wolf, A. Baer, Z. Vager, D. Zajfman, and V. Kh. Liechtenstein, Nucl. Instrum. Methods Phys. Res. B **168**, 268 (2000).
[21] A. Messiah, *Quantum Mechanics* (North-Holland, Amsterdam, 1963), Vol. 2.
[22] D. Zajfman, G. Both, E. P. Kanter, and Z. Vager, Phys. Rev. A **41**, 2482 (1990).
[23] D. Zajfman, T. Graber, E. P. Kanter, and Z. Vager, Phys. Rev. A **46**, 194 (1992).
[24] Z. Amitay, A. Baer, M. Dahan, J. Levin, Z. Vager, D. Zajfman, L. Knoll, M. Lange, D. Schwalm, R. Wester, A. Wolf, I. F. Schneider, and A. Suzor-Weiner, Phys. Rev. A **60**, 3769 (1999).
[25] H. Kreckel, S. Krohn, L. Lammich, M. Lange, J. Levin, M. Scheffel, D. Schwalm, J. Tennyson, Z. Vager, R. Wester, A. Wolf, and D. Zajfman, Phys. Rev. A **66**, 052509 (2002).
[26] R. Garcia-Molina, I. Abril, S. Heredia-Avalos, L. Lammich, H. Buhr, H. Kreckel, S. Krohn, D. Strasser, R. Wester, A. Wolf, D. Zajfman, and D. Schwalm, Nucl. Instrum. Methods Phys. Res., Sect. B **230**, 41 (2005).
[27] H. Bruhns, H. Kreckel, K. A. Miller, X. Urbain, and D. W. Savin, Phys. Rev. A **82**, 042708 (2010).
[28] K. A. Miller, H. Bruhns, M. Čížek, J. Eliášek, R. Cabrera-Trujillo, H. Kreckel, A. P. O'Connor, X. Urbain, and D. W. Savin, Phys. Rev. A **86**, 032714 (2012).
[29] W. Kolos and L. Wolniewicz, J. Chem. Phys. **43**, 2429 (1965).